Regular Article

PHYSICAL CHEMISTRY RESEARCH
Published by the
Iranian Chemical Society
www.physchemres.org
info@physchemres.org

Phys. Chem. Res., Vol. 12, No. 4, 949-962, December 2024
DOI: 10.22036/pcr.2024.422704.2441

Methylene Blue Adsorption on Modified Biochar with Magnetic Nanoparticles and Humic Acid Coating

Z. Sabrpisheh, E. Ghasemian Lemraski*, Z. Abbasi and Z. Tahmasebi

Department of Chemistry, Faculty of Science, Ilam University, P. O. Box: 69315516, Ilam, Iran

(Received 28 October 2023, Accepted 16 June 2024)

In this project, we modified the biochar adsorbent using iron oxide nanoparticles coated with humic acid to remove methylene blue, a cationic dye. The prepared adsorbent was characterized *via* different instrumental methods, such as Fourier-transform infrared spectroscopy (FT-IR), Brunauer-Emmett-Teller surface area measurement (BET), scanning electron microscopy (SEM), X-ray diffraction (XRD), and thermal gravimetric analysis (TGA). The presence of Fe_3O_4 nanoparticles was confirmed by vibrating sample magnetometer (VSM). Surface adsorption studies have been used to determine the factors influencing the surface adsorption of methylene blue by the prepared biochar adsorbent in aqueous environments. Different factors such as pH, mixing time, amount of adsorbent, and methylene blue concentration, have been noticed. The obtained data from removal experiments at different times and concentrations showed that the removal process is in accordance with the Langmuir isotherm and the Elovich kinetic equation. The isotherm parameters for surface adsorption were also determined.

Keywords: Humic acid, Adsorption, Azo dye, Isotherm, Biochar

INTRODUCTION

Water treatment is of paramount importance for several reasons, as it plays a critical role in ensuring the availability of clean, safe, and potable water for human consumption and various industrial and agricultural purposes. Access to uncontaminated and secure drinking water is crucial for maintaining human health. Contaminated water can carry harmful organisms (such as bacteria, viruses, and parasites) and stable contaminants (like inorganic and organic compounds) that can cause waterborne diseases. Effective water treatment processes help remove or inactivate these contaminants, reducing the risk of illnesses and improving public health. Water treatment techniques encompass a diverse array of processes and techniques designed to purify and enhance the quality of water for a multitude of purposes, encompassing drinking, industrial applications, and environmental conservation [1-3]. Coagulation and flocculation, sedimentation, filtration: disinfection, reverse osmosis, ion exchange, adsorption, membrane bioreactors, advanced oxidation processes, and electrocoagulation are some common water treatment methods [4-7].

Adsorption on biochar is a water treatment and environmental remediation technique that involves the using of biochar as one of the best adsorbent materials to remove water and soil contaminants. Biochar is a type of charcoal produced through the pyrolysis of biomass, such as wood, agricultural waste, or other organic materials, in a low or zero-oxygen environment. This process involves heating the biomass to high temperatures (typically between 350 °C and 700 °C) in a controlled manner, which results in the production of a stable form of carbon-rich material known as biochar. The choice of modification way depends on the target contaminants, the determining adsorption capacity, and the specific application [8-11]. Biochar offers a sustainable and cost-effective solution for environmental remediation by utilizing renewable biomass resources and converting waste materials into valuable products that

*Corresponding author. E-mail: e.ghasemian@ilam.ac.ir

contribute to ecosystem health and human well-being.

The modification process is often tailored to address the unique challenges posed by different types of pollutants and environmental conditions. Chemical activation, steam activation, acid and base treatment, oxidation, metal impregnation, and biomass source variation have been used to modify the biochar surface. In this study, we try to modify the surface of biochar by using humic acid and magnetic nanoparticles [12-16].

Humic acid (HA), a naturally occurring organic compound found in soil and water, can enhance the performance of activated carbon in several ways. In general, the modification of activated carbon by humic acid is an important strategy to enhance its adsorption capacity, selectivity, and overall performance in water and wastewater treatment [17]. This approach can contribute to more efficient and cost-effective solutions for removing water pollution and improving water quality in various settings. Humic acids are known to adsorb onto the surfaces of iron oxides like Fe_3O_4. This adsorption occurs through various mechanisms, including electrostatic attraction, hydrogen bonding, and coordination of functional groups on HA with iron situation on the Fe_3O_4 surface. The adsorption of HA onto Fe_3O_4 can change the surface functional group and reactivity of the iron oxide. The obtained composite has been used to remove methylene blue from water. Kinetic and isotherm data helped us to determine the details of interaction and adsorption. Fast adsorption and high adsorption capacity are the most important factors of the prepared adsorbent.

MATERIALS AND METHODS

The preparation of magnetic/humic acid/biochar composites involves combining magnetic nanoparticles, humic acid, and biochar to create a hybrid material with unique properties, such as enhanced adsorption capabilities and environmental applications.

Materials

All chemicals used to prepare the composite: biochar collected from oak forests in Ilam province, ferric chloride ($FeCl_3$), ferrous chloride ($FeCl_2$), ammonia, nitric acid (purity 65%), humic acid, and methylene blue dye were purchased from Merck, Germany.

Structural Analysis

Microscopic images of the prepared composite were obtained by Field Emission Scanning Electron Microscopy (FESEM, MIRA III, TESCAN Company, Czech). The crystalline structure of the nanocomposite was determined using an X-ray diffractometer (PW1730, PHILIPS Company, Netherlands). Fourier transform infrared (FTIR) spectroscopy was performed using a Bruker–Germany VBRTEX70 spectrometer. The absorption of the sample was determined by UV-visible spectrophotometer (Cary 300, UK). The surface area was determined using a micrometric surface area analyzer (Belsorp-miniII, BEL, Japan). The magnetic properties of the composite were determined *via* a vibrating-sample magnetometer (VSM MDKB, Danesh Pasch Magnetic Co. Kashan, Iran). The Fe measurements of the samples were performed using an ICP-MS NexION 300x instrument (Perkin Elmer).

Preparation

For the preparation of the adsorbent, the raw material samples used in this experiment were prepared from the oak forests of Ilam province. After being collected, they were dried at a temperature of 80 ºC and then converted into biochar for 3 h between 300-600 ºC inside an electric furnace under oxygen-free conditions.

Synthesis of core-shell composite. Initially, dissolve 2 g of ferric chloride ($FeCl_3$) in 50 ml of deionized water in a three-necked flask under vigorous stirring at a temperature of 90 °C. While stirring continuously, add ammonia dropwise until the pH of the mixture reaches 10. Next, add 1 g of humic acid to the solution and reflux it at 80 °C for 2 h. The resulting core-shell composite is separated and washed multiple times with distilled water and then dried at 80 °C for 12 h.

COOH/biochar. 5.2 g of biochar mixed with 100 ml of HNO_3 and stirred vigorously for 12 h under magnetic stirring. After 12 h, wash the precipitate with deionized water until the pH becomes neutral. Dry the obtained residue at 60 °C for 10 h. Then 8.1 g of the desired core-shell composite and disperse it in 500 ml of deionized water under ultrasonic waves for 30 min.

Finally, the desired humic acid/Fe_3O_4 nanoparticles are dispersed in 50 ml of deionized water under microwave irradiation for 30 min. In a separate container, disperse 8.1 grams of COOH/biochar in 50 ml of distilled water for

30 min. Afterward, gradually add the solution containing COOH/biochar to the initial solution, filter the resulting precipitate, and dry it at 80 °C for 24 h.

Experimental data collection. To prepare the methylene blue solution for adsorption study, initially, a stock solution of 500 ppm of methylene blue was used. The dye removal or adsorption experiments with varying initial concentrations, pH, mixing time, and adsorbent amount were performed. To adjust the pH within NaOH and HCl solutions. The removal percentage and adsorption efficiency for each experiment were calculated based on the following equation.

$$\%Dye\ removal = \frac{c_0 - c_t}{c_0} \times 100 \quad (1)$$

$$q_e = (c_0 - c_t)\frac{v}{m} \quad (2)$$

Where:

- C_0 is the dye concentration.
- Ce is the equilibrium dye concentration.
- C_t is the dye concentration at t.
- V is the volume of the solution.
- M is the amount of adsorbent.

RESULTS AND DISCUSSION

Characterization

FTIR (Fourier-transform infrared spectroscopy) of biochar shows valuable results related to chemical composition and structure. General main groups contain hydroxyl (OH), carbonyl (C=O), carboxyl (COOH), aromatic C=C bonds, and aliphatic C-H bonds. Peaks in the spectrum correspond to vibrations of these functional groups. Fe_3O_4 is a metal oxide with FCC unit cell structure, where (Fe^{3+}Otetrahedral), (Fe^{2+} octahedral), and (Fe^{3+} octahedral) O4 show different oxidation Fe cation [33-37]. So it's expected to see three different characteristic Fe-O peaks in FTIR spectrum before 1000 cm^{-1}. Figure 1 displayed a clear band of prepared Fe_3O_4 without any additional peak due to the precision in the preparation stages. The peak at 442 cm^{-1} is related to overlapping Fe–O stretching vibration mode with the octahedral structure and O_2 at 583 cm^{-1} is pointed to Fe–O bending vibration in octahedral structure. The prepared modified biochar shows a broad peak in the region of

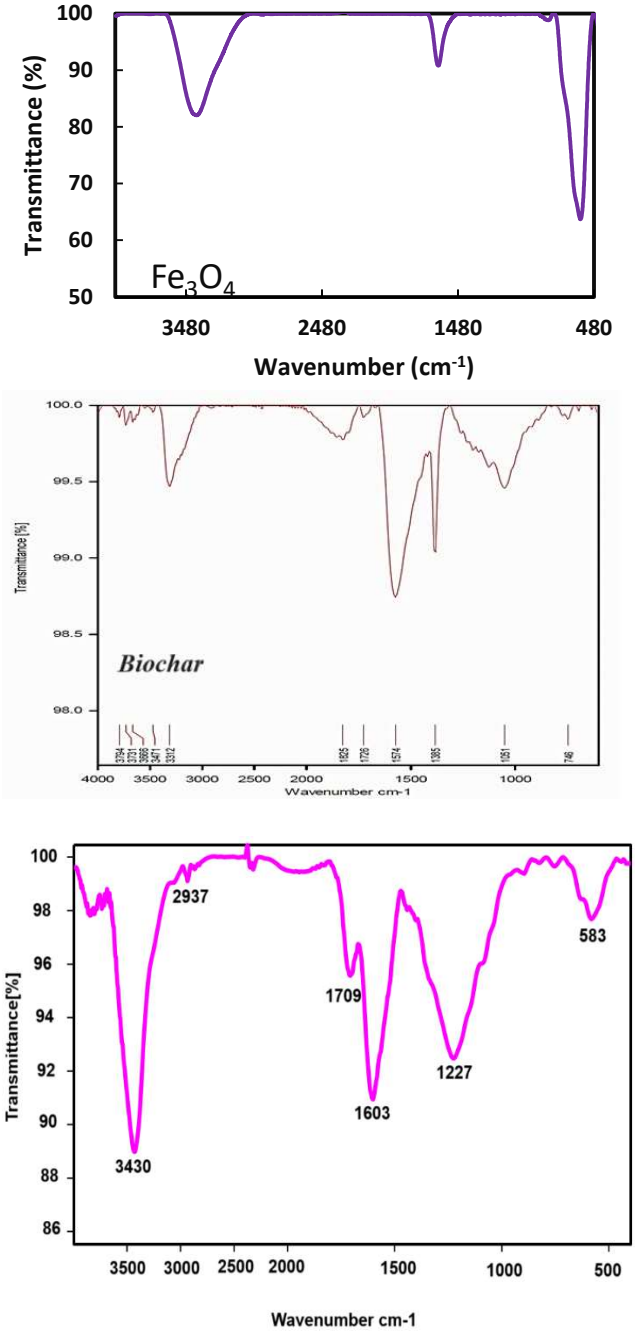

Fig. 1. FTIR spectrum of Fe_3O_4, biochar, and modified biochar.

3430 cm^{-1} indicative of O-H stretching vibrations from hydroxyl groups and water adsorbed on humic acid. Spectra in the region of 2937 cm^{-1} is associated with C-H stretching vibrations from aliphatic groups. The presence of carboxylic

acid functional groups can be confirmed by peaks in the range of 1600-1700 cm^{-1}, which correspond to C=O stretching vibrations of carboxylate groups. Biochar may show characteristic peaks associated with various functional groups present in the organic matter [18]. These can include peaks in the 2800-3000 cm^{-1} region for C-H stretching vibrations and peaks in the 1227 cm^{-1} range for C=C and C-H bending vibrations. Fe_3O_4 nanoparticles may exhibit characteristic peaks in the region of 400-700 cm^{-1} due to Fe-O stretching vibrations [19]. Figure 2 shows the TGA of the prepared adsorbent. It consists mainly of carbon, but it can also contain ash and other volatile components depending on the feedstock and pyrolysis conditions. When conducting TGA on biochar, a small sample is placed in a crucible and subjected to a controlled temperature ramp-up. As the temperature increases, biochar undergoes several stages of weight loss. These stages correspond to the decomposition of various organic components present in the biochar. The primary weight loss steps include the removal of water, volatile organics, and the breakdown of organic matter. The temperature at which significant weight loss occurs can indicate the thermal stability of the biochar. Biochar is generally stable at higher temperatures, making it a good candidate for pollutant treatment [20].

The surface porosity of the material plays a critical role in removal. A higher surface area provides more sites for molecules or ions to adhere to, increasing the adsorption capacity. Data in Table 1 revealed the BET analysis results and data. The provided data suggests the composite being analyzed showed a high specific surface area (873.41 [m^2 g^{-1}]), indicating that it is likely porous and has a significant surface available for adsorption. The total pore volume and mean pore diameter data provide additional insights into the pore size distribution of the material.

The specific shape and characteristics of adsorption and desorption isotherms for common biochar will depend on factors such as the feedstock used to produce the biochar, the pyrolysis conditions, and the surface structure of the prepared modified biochar (*e.g.*, size, charge, hydrophobicity). The Type II isotherm in Fig. 1C is commonly observed in porous materials like activated carbon, zeolites, and, in this context, biochar. It implies that the biochar has a porous structure with varying pore sizes that allow for multilayer adsorption. The hysteresis loop often seen in Type II isotherms suggests that

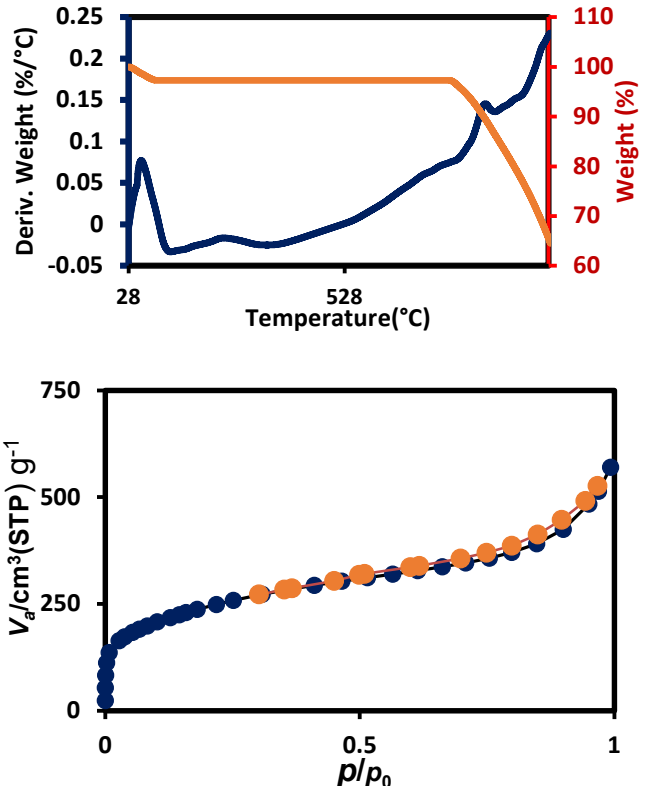

Fig. 2. TGA and N_2 adsorption/desorption diagram of modified biochar.

Table 1. N_2 Adsorption/desorption Analysis Data and Results

BET plot	
V_m	200.67 [cm^3(STP) g^{-1}]
$a_{s, BET}$	873.41 [m^2 g^{-1}]
Total pore volume (p/p_0 = 0.990)	0.872 [cm^3 g^{-1}]
Mean pore diameter	3.9936 [nm]

desorption requires more energy and is less reversible than adsorption [21].

Figure 3 shows FESEM images of modified biochar. A FESEM image of biochar would show the surface morphology of the material at a very high magnification. Biochar is a porous and carbonaceous material, and a FESEM image would reveal the rough and irregular surfaces. The FESEM image would capture the surface texture at a nanoscale or microscale level.

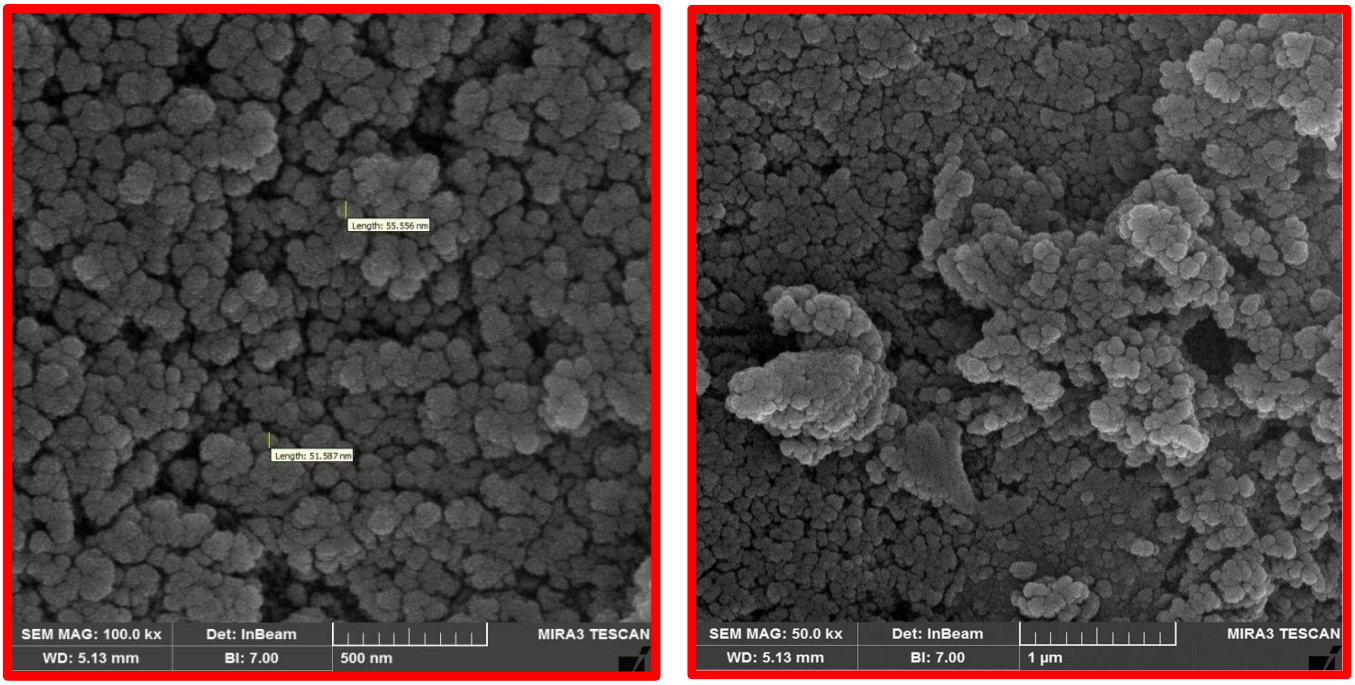

Fig. 3. FESEM images of modified biochar.

Figure 4 shows the X-ray diffraction (XRD) pattern for the prepared materials. Biochar often shows a broad hump centered around 2θ values between 20° and 30°, indicating the presence of amorphous carbon. This peak reflects the disordered structure of carbonaceous materials resulting from the pyrolysis process.

Magnetite (Fe_3O_4) typically shows multiple peaks at various angles (2θ) due to its crystalline structure. One of the prominent peaks for magnetite occurs around 2θ = 38 degrees. This peak corresponds to the (220) plane of magnetite. Another peak at 2θ = 75.5 degrees in an X-ray diffraction (XRD) pattern can be indicative of a specific crystallographic plane for a material. In the case of magnetite (Fe_3O_4), this peak corresponds to the (440) plane of magnetite [22]. When analyzing biochar using XRD, you may see a broad, diffuse hump on the XRD pattern without distinct peaks. This hump is characteristic of amorphous or disordered carbonaceous materials. The absence of sharp peaks is due to the absence of regular, repeating crystalline structures in biochar. Biochar with carbon-based structure, and it typically lacks well-defined crystalline structures. Instead, it contains amorphous carbon and may have some disordered arrangements. As a result, the XRD pattern for biochar is usually broad and featureless, which indicates its lack of crystallinity [23].

VSM data in Fig. 5 shows how the magnetization of the material changes as the magnetic field is increased and then decreased (a full magnetic hysteresis loop). As the magnetic field is increased from 0 to 10,000 Oe (Oersteds), the magnetization of the sample increases, indicating that the material is becoming magnetized in the direction of the applied field. When the magnetic field is reduced from 10,000 Oe back to 0 Oe, the magnetization does not return to zero, indicating that some residual magnetization remains in the material. This is characteristic of a ferromagnetic material like magnetite. The kind of the hysteresis loop provides results about the magnetic properties of the material, including its coactivity (the field strength at which it becomes magnetized) and its saturation magnetization (the maximum magnetization it can achieve under a strong magnetic field) [24].

Surface Adsorption Results

Adsorption is a process where components adhere to the surface of a solid or liquid, forming a thin film or layer. Various parameters influence adsorption processes , and

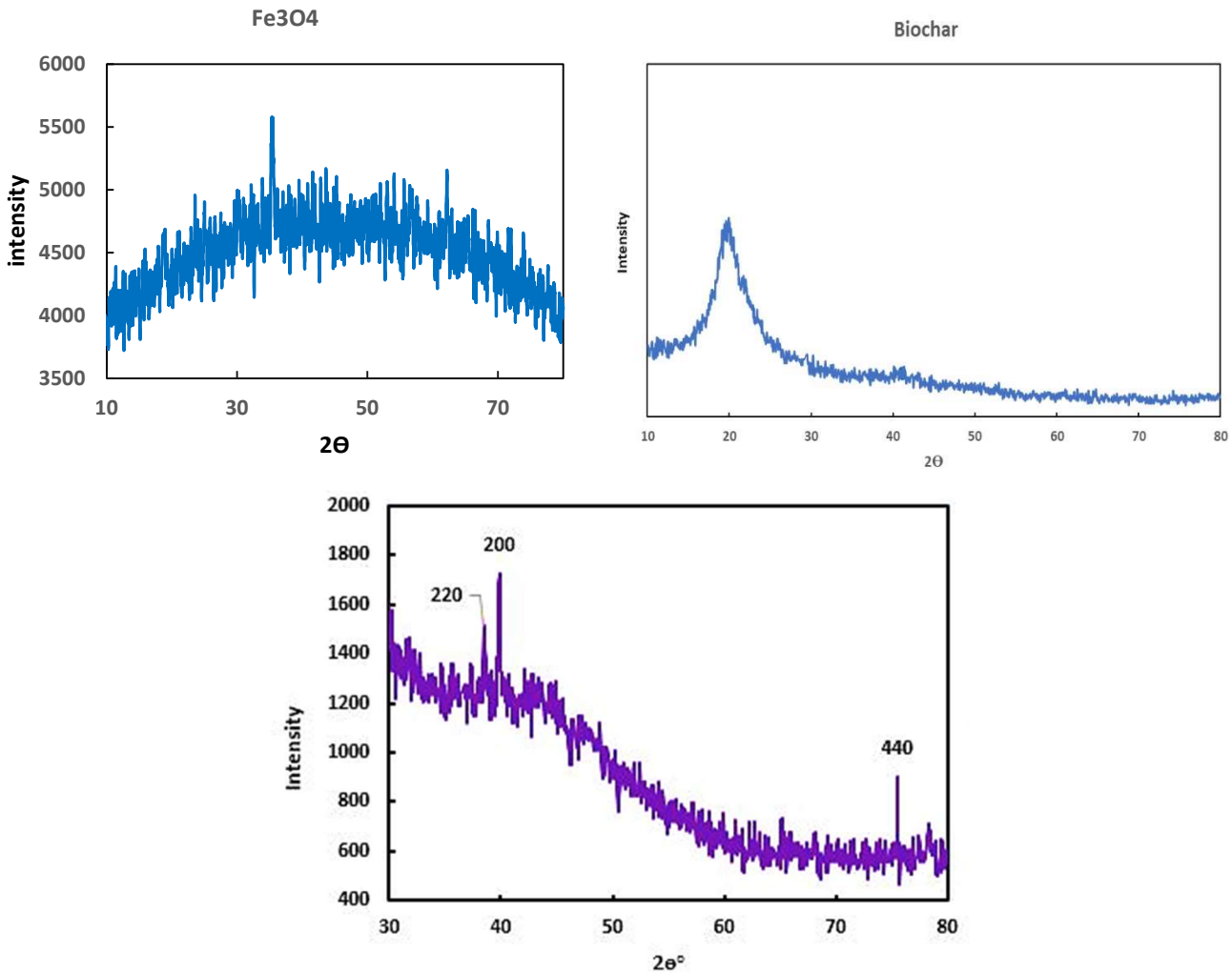

Fig. 4. XRD patterns of all the prepared sample.

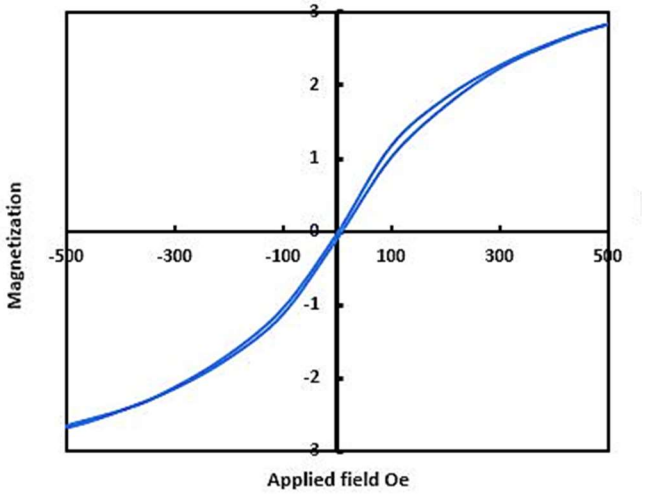

Fig. 5. VSM graph of modified biochar.

understanding these parameters is crucial for optimizing adsorption systems for specific applications. Understanding and optimizing these parameters is essential for designing effective adsorption processes for various applications, including water purification, gas separation, and adsorbent-based technologies like carbon-based filters and chromatography columns.

To optimize the removal of solutes through adsorption, it's essential to carefully consider the initial concentration, especially in the context of the specific adsorption system and its objectives. This may involve determining the removal ability of the adsorbent, evaluating the breakthrough behavior, and assessing the overall efficiency and feasibility of the process under varying initial concentration conditions.

Based on Fig. 6 a higher initial concentration of adsorbent in bulk leads to a higher adsorption capacity, assuming that the adsorbent has not reached saturation. This means that at higher initial concentrations, more solute molecules will be adsorbed onto the adsorbent until the available adsorption sites are filled. As the initial concentration increases, the amount adsorbed increases until a point of saturation is reached. Beyond this point, further increases in initial concentration may not significantly increase adsorption [25].

The influence of time on the removal of a dye *via* activated carbon-based materials is an important aspect to consider in the study of adsorption kinetics. Understanding how the adsorption process evolves over time helps in optimizing adsorption systems, predicting adsorption behavior, and determining the equilibrium adsorption capacity. The adsorption process typically follows a time-dependent pattern characterized by several stages: Initial rapid adsorption, transition to slower adsorption, and approaching equilibrium. As can be seen in Fig. 7 the dye concentration decreases rapidly at the beginning and then gradually until reaches a steady state or equilibrium, indicating that the removal process has reached a balance where removal and reintroduction (if any) are occurring at the same rate [26].

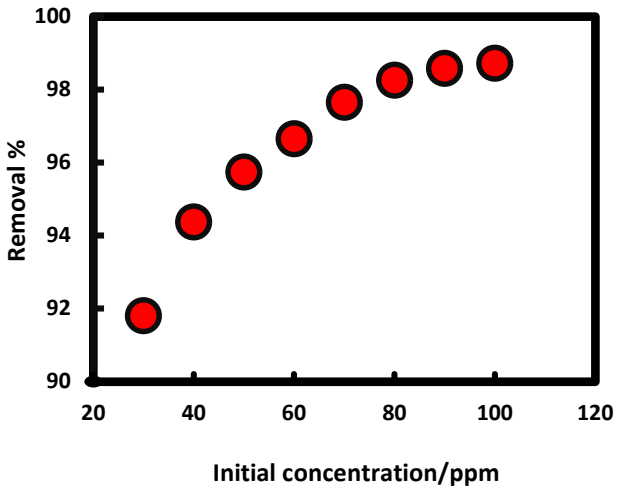

Fig. 6. The effect of the initial concentration on the removal of MB by modified biochar (pH = 6, adsorbent amount:0.2 g, 120 min).

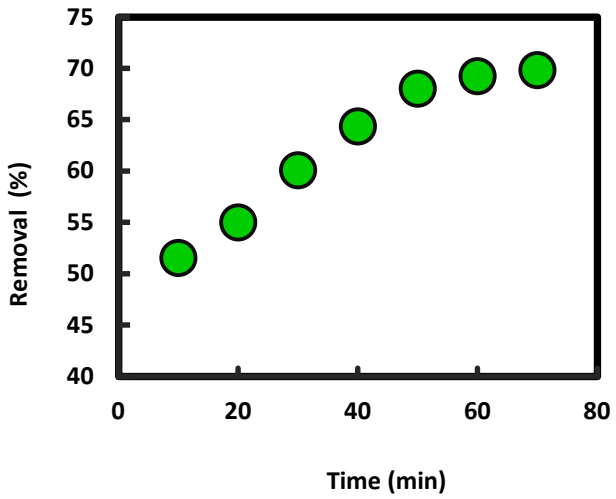

Fig. 7. The effect of contact time on the removal of MB on modified biochar (pH = 6, adsorbent amount: 0.2 g, 80 ppm).

The quantity of adsorbent plays an important role, particularly in the adsorption capacity. An increase in the amount of adsorbent typically results in a higher adsorption capacity. This occurs because accessible adsorption sites for solute components to bond with increase. Consequently, employing a larger amount of adsorbent proves advantageous when dealing with solutions characterized by high solute concentrations or when aiming for a high degree of pollutant removal. Furthermore, augmenting the quantity of adsorbent can expedite the attainment of adsorption equilibrium. A higher porosity and an enhanced amount of available adsorption sites contribute to a quicker establishment of equilibrium within the system. This becomes particularly vital in dynamic adsorption processes where shorter residence times are preferred. To investigate the impact of adsorbent dosage, we conducted surface adsorption experiments using consistent MB concentrations while varying the quantity of adsorbent, as presented in Fig. 8 In this scenario, we observed that the adsorption of methylene blue (MB) initially enhanced *versus* adsorbent dose rose, but subsequently decreased with further increments in the adsorbent amount. This behavior may be attributed to the enhanced availability of surface-active sites when the adsorbent amount is low. However, this pattern shifted when larger quantities of the adsorbent were employed. This change could be attributed to an augmentation in the surface

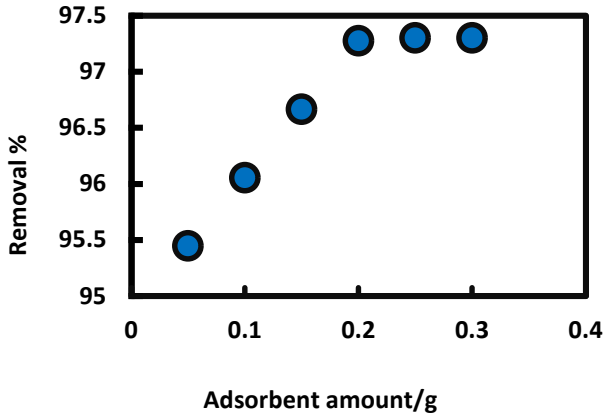

Fig. 8. The effect of the adsorbent amount on the adsorption process of MB on modified biochar (pH = 6, 80 ppm: 0.2 g of adsorbent, 120 min).

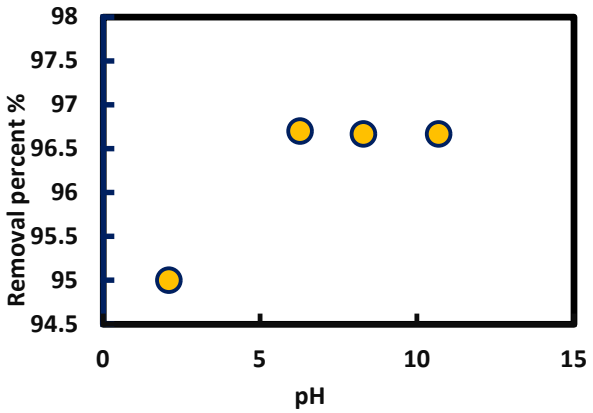

Fig. 9. Effect of pH on the removal of MB on modified biochar (80 ppm, adsorbent amount 0.2 g, 120 min).

sites of the adsorbent at higher doses, consequently resulting in a reduction in the rate of dye removal [27].

The pH of a mixture can have an important effect on the removal of methylene blue or any other dye onto the surface of the material. The removal behavior of methylene blue is changed due to the pH variation. Some key factors that influence pH include adsorbent surface charge, dye ionization, electrostatic interactions, chemical reactions, the presence of competing ions, adsorption capacity, and optimal pH. The effect of mixture pH on the adsorption experiments was investigated across a pH range of 1.0-10.0, as illustrated in Fig. 9. These results are a reflection of several factors, including electrostatic forces of dye compounds and polar surface sites, the charge on the modified biochar surface, the extent of dye ionization, and the presence of other ions in the solution. Figure 7 demonstrates a rapid increase in methylene blue (MB) removal at pH 5.5, followed by a decline in the pH range of 6.0 to 10.0. The modified biochar's surface carries a positive charge at acidic pH levels, causing the high removal ability for MB. Conversely, as the pH increases, the modified biochar surface contains negative charge due to the adsorption of OH- groups. This shift in charge contributes significantly to the decreased adsorption rate [30].

When biochar is modified with humic acid and Fe_3O_4 nanoparticles, the surface charge characteristics can undergo significant changes, impacting its adsorption behavior, stability, and interaction with surrounding ions or molecules. Humic acid is composed of organic components with carboxyl, phenolic, and hydroxyl functional groups. These functional groups can ionize in water, causing to the making negatively charged sites on the biochar surface. Therefore, the addition of humic acid can increase the negative charge density on the biochar surface related to the presence of carboxyl and phenolic groups, which tend to dissociate at neutral or acidic pH. Iron oxide nanoparticles, such as Fe_3O_4, are often used to confer magnetic properties to biochar, enabling easier separation and recovery from aqueous solutions. The Fe_3O_4 nanoparticles themselves may be negative, depending on the pH and surface functionalization. When immobilized on the biochar surface, they can contribute to the overall surface charge of the prepared sample. The surface charge of modified biochar can vary with pH due to the protonation/deprotonation of surface groups located on the components. At acidic pH, carboxyl and hydroxyl groups may become protonated, leading to a decrease in negative surface charge. Conversely, at higher pH values, these groups tend to deprotonate, resulting in an increase in negative surface charge. The pH of the mixture can affect both the polarity of the modified biochar and the ionization state of methylene blue. At lower pH values, the biochar surface may carry a lower negative charge or even become positively charged due to the adsorption of proton of the surface groups. This can reduce the electrostatic interaction between biochar and MB, leading to decreased adsorption efficiency. Conversely, at higher pH values, the surface charge of biochar becomes more negative, enhancing the electrostatic attraction for MB molecules.

Adsorption Isotherm

Adsorption isotherms are used to understand the relationship between the concentration of a solute (in this case, a dye) in a liquid phase and the amount of solute adsorbed on adsorbent at a specific temperature. The Langmuir [30], Freundlich [31], and Temkin [32], isotherms yield crucial parameters, including absorption capacity, adsorption type (whether physical or chemical), surface homogeneity, and interaction energy.

The Langmuir isotherm is a model used to describe the adsorption of gas molecules onto a solid surface. It assumes a monolayer coverage of adsorbate molecules on the surface and is based on the assumption that adsorption only occurs at specific sites on the surface. The Langmuir isotherm equation is typically expressed as:

$$\frac{C_e}{q_e} = \frac{1}{K_L q_m} + \frac{C_e}{q_m} \quad (3)$$

where K_L is the equilibrium constant related to the adsorption process (l mg^{-1}), and q_m is the theoretical maximum adsorption capacity (mg g^{-1}). The values of q_m and K_L were obtained via a plot of C_e/q_e *vs*. C_e. The calculated results are given in Table 2.

The Freundlich isotherm is another model used to describe adsorption onto a solid surface, particularly when the surface is heterogeneous and multilayer adsorption occurs. Unlike the Langmuir isotherm, which assumes monolayer adsorption on a homogeneous surface, the Freundlich isotherm allows for multiple layers of adsorbate molecules and considers non-ideal surface conditions. The Freundlich isotherm equation is as follows:

$$\log q_e = \log K_f + \frac{1}{n} \log C_e \quad (4)$$

n and K_f are the Freundlich parameters proper to the adsorption intensity and relative adsorption capacity of the adsorbent, respectively. In some research, the value of n has been applied to reveal the physical or chemical of the adsorption process. Also, the ratio of 1/n provides homogeneity or heterogeneity of the surface active sites. The extrapolated data from Eq. (4) in Table 2 show that the adsorption of MB on the nanocomposite is physical and the Freundlich isotherm failed to describe the adsorption process.

Table 2. Isotherm Constant and Correlation Coefficients Calculated for MB Adsorption

Isotherm	Parameters	
Langmuir	Q_m (mg/g)	143.71
	K_a (l mg^{-1})	0.01
	R^2	0.99
Freundlich	$1/n$	0.58
	K_f (l mg^{-1})	2.44
	R^2	0.95
Tempkin	B_1	17.9
	K_T (l mg^{-1})	1.74
	R^2	0.85

The Temkin isotherm is a model used to describe adsorption on solid surfaces, taking into account interactions between adsorbate molecules and the surface. It assumes that the heat of adsorption decreases linearly with the coverage of the surface. This is in contrast to the Langmuir isotherm, which assumes a constant heat of adsorption, and the Freundlich isotherm, which assumes a logarithmic decrease. Temkin parameters can be obtained from the plot of q_e against ln C_e based on the linear form of the Temkin isotherm as seen in Eq. (6).

$$q_e = B \ln A + B \ln C_e \quad (5)$$

Based on Table 2 these isotherms can help in estimating adsorption capacity, affinity, and the mechanism of adsorption. The selection of the suitable isotherm model depends on the specific adsorbent-dye system and the nature of the adsorption process, and it is often determined through statistical analysis and curve fitting of experimental data. By comparing the experimental adsorption capacity values with the extrapolated data from all four isotherms presented in Table 2, it was determined that the Langmuir isotherm is the best choice for investigating the dye absorption onto the biochar. The parameters indicated that the adsorption of MB onto the biochar is in accordance with Langmuir model, occurred at homogeneous surface sites, and resulted in a monolayer formation on the surface of the surface [33].

The addition of humic acid (HA) to the surface of biochar can serve several important roles in modifying its properties and enhancing its efficiency as an adsorbent for substances like methylene blue. Humic acid with polar group can interact with the surface of biochar through chemical bonding, hydrogen bonding, or electrostatic interactions, leading to the functionalization of the biochar surface. This functionalization can increase the adsorption capacity of biochar. Humic acid has buffering properties, which can help maintain the pH of the solution within a certain range during the adsorption process. This is particularly important for adsorption experiments where pH can affect the ionization state of both the adsorbate (*e.g*., methylene blue) and the adsorbent (modified biochar). By stabilizing the pH, humic acid ensures that the adsorption conditions remain optimal for efficient adsorption of methylene blue onto modified biochar Humic acid molecules can form complexes with methylene blue through π-π interactions, hydrogen bonding, or electrostatic interactions, facilitating its adsorption onto the modified biochar surface. This synergistic interaction between humic acid and methylene blue enhances the overall adsorption performance of the modified biochar. Humic acid contains negatively charged functional groups, such as carboxyl groups, which can increase the negative surface charge density of biochar. This modification of the surface charge can influence the electrostatic interactions between the modified biochar and positively charged molecules like methylene blue. The increased negative surface charge can enhance the electrostatic attraction of methylene blue molecules to the modified biochar surface, thereby improving adsorption efficiency. Humic acid can act as a dispersing agent, preventing agglomeration or aggregation of Fe_3O_4 nanoparticles on the biochar surface. This ensures uniform distribution of Fe_3O_4 nanoparticles and prevents their precipitation or settling during the adsorption process. Additionally, humic acid can stabilize Fe_3O_4 nanoparticles by providing steric hindrance and preventing their agglomeration, thereby maintaining their magnetic properties and facilitating the separation of modified biochar from the aqueous solution after adsorption. Overall, the addition of humic acid to the surface of biochar plays a crucial role in enhancing its adsorption performance by facilitating surface functionalization, pH buffering, enhancing sorption capacity, modifying surface charge, and stabilizing Fe_3O_4 nanoparticles. These effects collectively contribute to the improved efficiency and effectiveness of modified biochar as an adsorbent for pollutants like methylene blue.

Adsorption Kinetics

The kinetic equation used to describe the rate at which a dye is removed or adsorbed from a liquid phase onto a solid adsorbent is typically modeled using one of several kinetic models. The most commonly used kinetic models for dye removal include the pseudo-first-order and pseudo-second-order kinetics. Here's an explanation of both:

The pseudo-first-order kinetic model is a simplified approach often used to describe the kinetics of adsorption processes, particularly in the context of surface adsorption onto solid adsorbents. It assumes that the rate-limiting step of the adsorption process is the transfer of the adsorbate from the solution phase to the surface of the adsorbent [33,34].
It can be expressed as:

$$\log(q_e - q_t) = \log(q_e) - \frac{k_1}{2.303\ t} \quad (6)$$

where q_e and q_t are the adsorption amount at equilibrium and at time t; and k_1 is the pseudo-first-order rate constant (min^{-1}). The values of k_1 and q_e can be calculated from the graph of $\log(q_e - q_t)$ against t, respectively. The results in Table 3 revealed that the present model cannot confirm the experimental data, considering the r values of R^2 and the fact that there is not any accordance between the experimental and the theoretical data.
The pseudo-second-order kinetic model assumes that the rate of dye removal is proportional to the square of the concentration of available adsorption sites on the adsorbent. It can be expressed as:

$$\frac{t}{q_t} = \frac{1}{k_2 q_e^2} + \frac{1}{q_e(t)} \quad (7)$$

Where k_2 is the second-order constant rate (g mg^{-1} min^{-1}). Based on obtained data of R^2, k_2, and q_e in Table 3, it finds the present model does not have the ability to correlate dye removal [35].

The Elovich equation is a kinetic model used to describe the adsorption process on solid surfaces, particularly for chemisorption or physisorption phenomena where the

adsorbate interacts strongly with the adsorbent surface. This model accounts for the variation of adsorption rate over time, reflecting the gradual decrease in available adsorption sites on the surface. The linear form of this model in Eq. (9) contains q_t (the amount of adsorbed component at time, *t*,) α (the initial adsorption rate (mg g^{-1} min^{-1})), and β (the desorption constant (g mg^{-1}) during any experiment) [36,37].

$$q_t = \frac{1}{\beta}\ln(\alpha\beta) + \frac{1}{\beta}\ln(t) \quad (8)$$

Based on the extrapolated data in Table 3, it can be seen that the removal of MB on modified biochar is confirmed by the Elovich model. It is observed that the Elovich model can be used to describe the adsorption of MB on modified biochar while other kinetic models do not.

The last used model in this research for the kinetics study of adsorption is the intra-particle diffusion model. Based on this model, the rate of adsorption undergoes adsorbent diffusion in two steps: the concentration gradients of matter between the bulk and the film around the adsorbent, as well as the concentration gradient between the film around the adsorbent and the surface pores [38]. The intra-particle diffusion model is revealed by Eq. (10):

$$q_t = K_{dif} t^{1/2} + C \quad (9)$$

Table 3. Calculated Kinetic Constant and Correlation Coefficients for MB Adsorption

Model	Parameter	
First-order	q_e(cal.)	65
	$K_1 \times 10^{-3}$ (l min^{-1})	54.35
	R^2	0.95
Second-order	q_e(cal.)	64
	$K_2 \times 10^{-3}$ (l min^{-1})	10.4
	R^2	0.85
	β	0.79
Elovich	α	5.85
	R^2	0.99
	K_{dif} (l min^{-1})	0.35
Intraparticle	C	33.64
	R^2	0.85

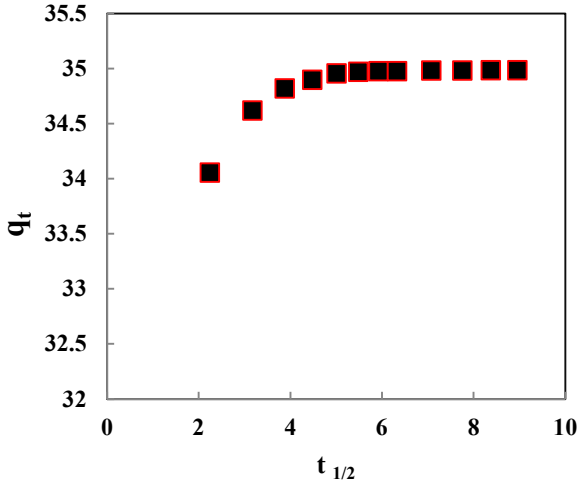

Fig. 10. Graph of q_t *vs.* $t_{1/2}$.

The values of K_{dif} and C were extracted from the plot of q_t *vs.* $t^{1/2}$ (Fig. 10) and the obtained values are reported in Table 3. The distance of R^2 values (Table 3) from unity showed the present model is not sufficient for the kinetic study of the adsorption.

CONCLUSION

This research revealed an experimental study of the preparation, characterization, and application of modified magnetic biochar. General characterization methods such as BET, scanning electron microscope (SEM), Fourier transform infrared spectroscopy (FT-IR), X-ray Diffraction (XRD), and thermo gravimetric analysis TGA/DTA, confirmed the significant changes in the surface structure of biochar during modification and functionalization. The N_2 adsorption data determined that the biochar completely contained microspores, confirming a high BET surface area of 800 m^2 g^{-1} and showing Type II isotherm. The experimental adsorption data exhibited the maximum adsorbed amount of 143 mg/g for methylene blue. The best adsorption percent has been observed at pH: 6.2, 60 min, 80 ppm of dye concentration, and 0.2 g of adsorbent. High efficiency in azo dye removal indicates that the modified biochar is a good candidate for water treatment and removal of pollution from the surrounding.

ACKNOWLEDGMENTS

The authors are grateful for the financial support from the Research Councils of Ilam University.

REFERENCES

[1] Kamgaing, T.; Doungmo, G.; Tchieno, F. M. M.; Kouonang, J. J. G.; Mbadcam, K. J., Kinetic and isotherm studies of bisphenol A adsorption onto orange albedo(*Citrus sinensis*): Sorption mechanisms based on the main albedo components vitamin C, flavones glycosides and carotenoids. *J. Environ. Sci. Health*, Part A, **2017**, *52* (8), 757-769. doi.org/10.1080/10934529.2017.1303315.

[2] Rashid, T., Sustainable wastewater treatment *via* dye-surfactant interaction: a critical review. *Ind. Eng. Chem. Res.,* **2020**, *59*, 9719-9745. doi.org/10.1021/acs.iecr.0c00676.

[3] Islam, M. A.; Islam, S. L.; Hassan, A., Impact of climate change on water with reference to the Ganges-Brahmaputra-Meghna River Basin. *J. Water Chem.* **2017**, 121-160. DOI: 10.1016/B978-0-12-809330-6.00003-9.

[4] Sharifi, F.; Ghasemian Lemraski, E; Sharafinia, S., Super hydrophobic PU sponge modified by poly-vinylidene fluoride/SBA-15@NPS hybrid, *Soft Materials*. **2023**, *22*, 41-53. doi.org/10.1080/1539445X.2023.2288585.

[5] Mburu, N.; Tebitendwa, S. M.; Rousseau, D. P.; Van Bruggen, J. J. A.; Lens, P. N., Performance evaluation of horizontal subsurface flow-constructed wetlands for the treatment of domestic wastewater in the tropics. *J. Environ Eng (New York)*. **2013**, *139* (3), 358-367. DOI: 10.1061/(ASCE)EE.1943-7870.00006.

[6] Padovan, R. N.; de Carvalho, L. S.; de Souza Bergo, P. L.;Xavier, C.; Leitão, A.; dos Santos Neto, Á. J.; Azevedo, E. B., Degradation of hormones in tap water by heterogeneous solar TiO_2-photocatalysis: Optimization, degradation products identification, and estrogenic activity removal. *J. Environ.Chem.Eng*., **2021**, *9* (6), 106442. DOI: 10.1016/j.jece.2021.106442.

[7] Nasution, M. A.; Yaakob, Z.; Ali, E.; Tasirin, S. M.; Abdullah, S. R. S., Electrocoagulation of palm oil mill effluent as wastewater treatment and hydrogen production using electrode aluminum. *J. Environ. Qual*. **2011**, *40* (4), 1332-1339. DOI: 10.2134/jeq2011.0002.

[8] Ahmad, M.; Rajapaksha, A. U.; Lim, J. E.; Zhang, M.; Bolan, N.; Mohan, D.; Ok, Y. S., Biochar as a sorbent for contaminant management in soil and water: a review. *Chemosphere*, **2014**, *99*, 19-33. DOI: 10.1016/ j.chemosphere.2013.10.071.

[9] Qiu, B.; Tao, X.; Wang, H.; Li, W.; Ding, X.; Chu, H., Biochar as a low-cost adsorbent for aqueous heavy metal removal: A review. *J Anal Appl Pyrolysis*. **2021**, *155*, 105081. DOI: 10.1016/j.jaap.2021.105081.

[10] Tan, X.; Liu, Y.; Zeng, G.; Wang, X.; Hu, X.; Gu, Y.; Yang, Z., Application of biochar for the removal of pollutants from aqueous solutions. *Chemosphere*. **2015**, *125*, 70-85. DOI: 10.1016/j.chemosphere.2014.12.058.

[11] Yaashikaa, P. R.; Kumar, P. S.; Varjani, S.; Saravanan, A., A critical review on the biochar production techniques, characterization, stability and applications for circular bioeconomy. *Biotechnol. Rep*. **2020**, *28*, e00570. DOI: 10.1016/j.btre.2020.e00570.

[12] Hou, J.; Yu, J.; Li, W.; He, X.; Li, X., The effects of chemical oxidation and high-temperature reduction on surface functional groups and the adsorption performance of biochar for sulfamethoxazole adsorption. *Agronomy*, **2022**, *12* (2), 510. DOI: 10.3390/ agronomy12020510.

[13] Li, Y.; Sheng, G.; Chiou, C. T., Impact of humic acid on the removal of heavy metals from aqueous solutions using carbonaceous sorbents. *Environ. Sci. Technol.* **2017**, *51*, 10431-10438. DOI: 10.1016/ j.scitotenv.2013.09.044.

[14] Zeghioud, H.; Fryda, L.; Djelal, H.; Assadi, A.; Kane, A., A comprehensive review of biochar in removal of organic pollutants from wastewater: Characterization, toxicity, activation/functionalization and influencing treatment factors. *J. Water Process. Eng*. **2022**, *47*, 102801. DOI: 10.1016/j.jwpe.2022.102801.

[15] Sachdeva, S.; Kumar, R.; Sahoo, P. K.; Nadda, A. K., Recent advances in biochar amendments for immobilization of heavy metals in an agricultural ecosystem: A systematic review. *Environ. Pollut*. **2023**, 120937. DOI: 10.1016/j.envpol.2022.120937.

[16] Ahuja, R.; Kalia, A.; Sikka, R.; P, C., Nano Modifications of Biochar to Enhance Heavy Metal Adsorption from Wastewaters: A Review. *ACS omega*. **2022**, *7* (50), 45825-45836.

DOI: 10.1021/ acsomega.2c05117.

[17] Hassaan, M. A.; El Nemr, A.; Elkatory, M. R.; Ragab, S.; El-Nemr, M. A.; Pantaleo, A., Synthesis, characterization, and synergistic effects of modified biochar in combination with α-Fe_2O_3 NPs on biogas production from red algae Pterocladia capillacea. *Sustainability*. **2021**, *13* (16), 9275. DOI: 10.3390/su13169275.

[18] Wang, C.; Tu, Q.; Dong, D.; Strong, P. J.; Wang, H.; Sun, B.; Wu, W., Spectroscopic evidence for biochar amendment promoting humic acid synthesis and intensifying humification during composting**.** *J. Hazard. Mater.* **2014**, *280*, 409-416. DOI: 10.1016/ j.jhazmat.2014.08.030.

[19] Yang, K.; Peng, H.; Wen, Y.; Li, N., Re-examination of characteristic FTIR spectrum of secondary layer in bilayer oleic acid-coated Fe_3O_4 nanoparticles. *Appl. Surf. Sci.* **2010**, *256* (10), 3093-3097. DOI: 10.1016/ j.apsusc.2009.11.079.

[20] Chen, T.; Cai, J.; Gong, D.; Liu, C.; Liu, P.; Cheng, X.; Zhang, D., Facile fabrication of 3D biochar absorbers dual-loaded with Fe3O4 nanoparticles for enhanced microwave absorption. *J. Alloys Compd*. **2023**, *935*, 168085. DOI: 10.1016/j.jallcom.2022.168085.

[21] Ravikovitch, P. I.; Domhnaill, S. Ó.; Neimark, A. V.; Schüth, F.; Unger, K. K., Capillary hysteresis in nanopores: theoretical and experimental studies of nitrogen adsorption on MCM-41. *Langmuir*, **1995**, *11* (12), 4765-4772. DOI: 10.1021/la00012a030.

[22] Nurdan, K. Y.; Fatma, K. B.; Koç, M. M.; Dilek, N., Characterization of magnetic Fe_3O_4@ SiO_2 nanoparticles with fluorescent properties for potential multipurpose imaging and theranostic applications. *J. Mater. Sci. Mater. Electron*. **2020**, *31* (20), 18278-18288. DOI: 10.1007/s10854-020-04375-7.

[23] Ibrahim, A. R.; Li, X.; Zhou, Y.; Huang, Y.; Chen, W.; Wang, H.; Li, J., Synthesis of spongy-like mesoporous hydroxyapatite from raw waste eggshells for enhanced dissolution of ibuprofen loaded via supercritical CO_2. *Int. J. Mol. Sci.* **2015**, *16* (4), 7960-7975. DOI: 10.3390/ijms16047960.

[24] Chen, W.; Li, X.; Xue, G.; Wang, Z.; Zou, W., Magnetic and conducting particles: preparation of polypyrrole layer on Fe_3O_4 nanospheres. *Appl. Surf. Sci.* **2003**, *218* (1-4), 216-222. DOI: 10.1016/S0169-4332(03)00590-7.

[25] Di, J.; Ruan, Z.; Zhang, S.; Dong, Y.; Fu, S.; Li, H.; Jiang, G., Adsorption behaviors and mechanisms of Cu^{2+}, Zn^{2+} and Pb^{2+} by magnetically modified lignite. *Sci Rep.* **2022**, *12* (1), 1394. DOI: 10.1038/s41598-022-05453-y.

[26] Bhat, S. A.; Zafar, F.; Mondal, A. H.; Mirza, A. U.; Haq, Q. M. R.; Nishat, N., Efficient removal of Congo red dye from aqueous solution by adsorbent films of polyvinyl alcohol/melamine-formaldehyde composite and bactericidal effects. *J. Clean. Prod.* **2020**, *255*, 120062. DOI: 10.1016/j.jclepro.2020.120062.

[27] Moradnejati, S.; Soleiman-Beigi, M.; Ghasemian Lemraski, E.; Baghelani, M., Synthesis and application of natural asphalt sulfonic acid (NA-SO_3H) as a novel and reusable carbonaceous super adsorbent for rapid decolorization of aqueous dye solutions, *Colloids and Surfaces A*: *Physicochemical and Engineering Aspects*, **2024**, 690, 133741, doi.org/10.1016/j.colsurfa.2024.133741.

[28] Bhat, S. A.; Zafar, F.; Mondal, A. H.; Kareem, A.; Mirza, A. U.; Khan, S.; Nishat, N., Photocatalytic degradation of carcinogenic Congo red dye in aqueous solution, antioxidant activity and bactericidal effect of NiO nanoparticles. *J. Iran. Chem. Soc.* **2020**, *17*, 215-227. DOI: 10.1007/s13738-019-01767-3.

[29] Mohammad, N.; Atassi, Y., Adsorption of methylene blue onto electrospun nanofibrous membranes of polylactic acid and polyacrylonitrile coated with chloride doped polyaniline. *Sci. Rep.* **2020**, *10* (1), 13412. DOI: 10.1038/s41598-020-69825-y.

[30] Langmuir, I., The Constitution and Fundamental Properties of Solids and Liquids. Part I Solids *J. Am. Chem. Soc*. **1916**, *38* (11), 2221-2295. DOI: 10.1021/ ja02268a002.

[31] Freundlich, H. M. F., Over the adsorption in solution. *J. Phys. Chem.*, **1906**, *57* (385471), 1100-1107.

[32] Temkin, M. J.; Pyzhev, V., *Acta Physiol. Plant. URSS.* **1940**, *12*, 217-222.

[33] Mahmoodi, N. M.; Mokhtari-Shourijeh, Z, aration and dye removal ability from wastewater. *Desalination Water Treat*. **2016**, *57* (42), 20076-20083. DOI: 10.1080/ 19443994.2015.1109562.

[34] Sharafinia, S.; Farrokhnia, A.; Ghasemian Lemraski, E., The adsorption of cationic dye onto ACPMG@ZIF-8

core-shell, optimization using central composite response surface methodology (CCRSM), *Colloids and Surfaces A: Physicochemical and Engineering Aspects*, **2022**, *634* (128039), doi.org/10.1016/j.colsurfa.2021.128039.

[35] Lagergren, S., Zur theorie der sogenannten adsorption geloster stoffe. Kungliga svenska vetenskapsakademiens. *Handlingar*. **1898**, *24*, 1-39.

[36] Ho, Y. S.; McKay, G., Pseudo-second order model for sorption processes. *Process Biochem*. **1999**, *34* (5), 451-465. DOI: 10.1016/S0032-9592(98)00112-5.

[37] Roginsky, S.; Zeldovich, Y. B., The catalytic oxidation of carbon monoxide on manganese dioxide.*Acta Phys. Chem. USSR*, **1934**, *1* (554), 2019. DOI: 10.4236/ aces.2013.34B003.

[38] G. Crank, The Mathematics of Diffusion, **1933**.